GOCE DELCEV UNIVERSITY - STIP
FACULTY OF COMPUTER SCIENCE

The journal is indexed in
EBSCO

ISSN 2545-4803 on line
DOI: 10.46763/BJAMI

BALKAN JOURNAL OF APPLIED MATHEMATICS AND INFORMATICS (BJAMI)

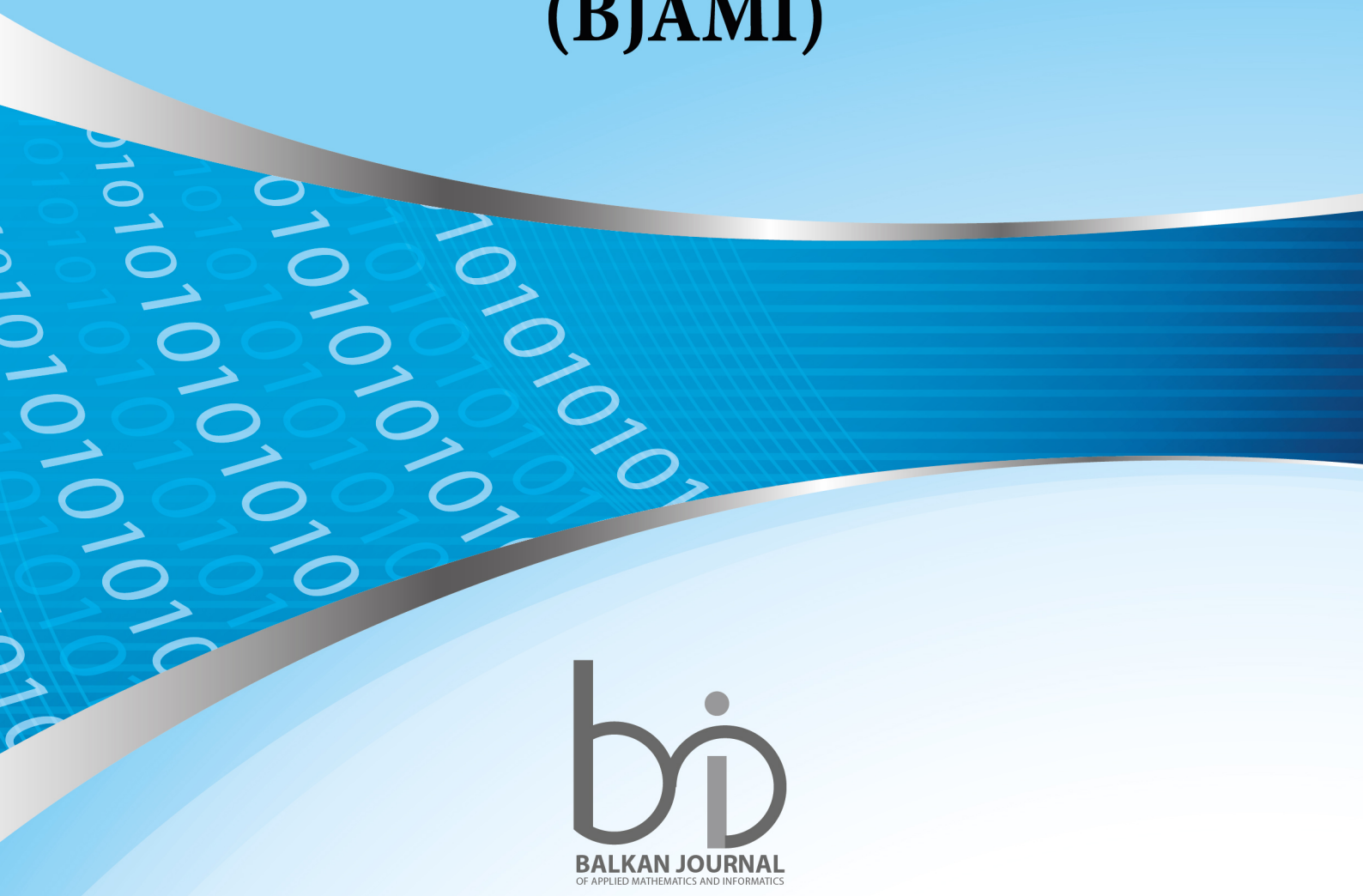

BALKAN JOURNAL
OF APPLIED MATHEMATICS AND INFORMATICS

YEAR 2022

VOLUME V, Number 1

GOCE DELCEV UNIVERSITY - STIP
FACULTY OF COMPUTER SCIENCE

ISSN 2545-4803 on line

BALKAN JOURNAL OF APPLIED MATHEMATICS AND INFORMATICS

(BJAMI)

YEAR 2022 VOLUME V, Number 1

AIMS AND SCOPE:
BJAMI publishes original research articles in the areas of applied mathematics and informatics.

Topics:
1. Computer science;
2. Computer and software engineering;
3. Information technology;
4. Computer security;
5. Electrical engineering;
6. Telecommunication;
7. Mathematics and its applications;
8. Articles of interdisciplinary of computer and information sciences with education, economics, environmental, health, and engineering.

Managing editor
Biljana Zlatanovska Ph.D.

Editor in chief
Zoran Zdravev Ph.D.

Lectoure
Snezana Kirova

Technical editor
Sanja Gacov

Address of the editorial office
Goce Delcev University – Stip
Faculty of philology
Krste Misirkov 10-A
PO box 201, 2000 Štip,
Republic of North Macedonia

BALKAN JOURNAL
OF APPLIED MATHEMATICS AND INFORMATICS (BJAMI), Vol 3

ISSN 2545-4803 on line
Vol. 5, No. 1, Year 2022

EDITORIAL BOARD

Adelina Plamenova Aleksieva-Petrova, Technical University – Sofia,
Faculty of Computer Systems and Control, Sofia, Bulgaria
Lyudmila Stoyanova, Technical University - Sofia , Faculty of computer systems and control,
Department – Programming and computer technologies, Bulgaria
Zlatko Georgiev Varbanov, Department of Mathematics and Informatics,
Veliko Tarnovo University, Bulgaria
Snezana Scepanovic, Faculty for Information Technology,
University "Mediterranean", Podgorica, Montenegro
Daniela Veleva Minkovska, Faculty of Computer Systems and Technologies,
Technical University, Sofia, Bulgaria
Stefka Hristova Bouyuklieva, Department of Algebra and Geometry,
Faculty of Mathematics and Informatics, Veliko Tarnovo University, Bulgaria
Vesselin Velichkov, University of Luxembourg, Faculty of Sciences,
Technology and Communication (FSTC), Luxembourg
Isabel Maria Baltazar Simões de Carvalho, Instituto Superior Técnico,
Technical University of Lisbon, Portugal
Predrag S. Stanimirović, University of Niš, Faculty of Sciences and Mathematics,
Department of Mathematics and Informatics, Niš, Serbia
Shcherbacov Victor, Institute of Mathematics and Computer Science,
Academy of Sciences of Moldova, Moldova
Pedro Ricardo Morais Inácio, Department of Computer Science,
Universidade da Beira Interior, Portugal
Georgi Tuparov, Technical University of Sofia Bulgaria
Dijana Karuovic, Tehnical Faculty "Mihajlo Pupin", Zrenjanin, Serbia
Ivanka Georgieva, South-West University, Blagoevgrad, Bulgaria
Georgi Stojanov, Computer Science, Mathematics, and Environmental Science Department
The American University of Paris, France
Iliya Guerguiev Bouyukliev, Institute of Mathematics and Informatics,
Bulgarian Academy of Sciences, Bulgaria
Riste Škrekovski, FAMNIT, University of Primorska, Koper, Slovenia
Stela Zhelezova, Institute of Mathematics and Informatics, Bulgarian Academy of Sciences, Bulgaria
Katerina Taskova, Computational Biology and Data Mining Group,
Faculty of Biology, Johannes Gutenberg-Universität Mainz (JGU), Mainz, Germany.
Dragana Glušac, Tehnical Faculty "Mihajlo Pupin", Zrenjanin, Serbia
Cveta Martinovska-Bande, Faculty of Computer Science, UGD, Republic of North Macedonia
Blagoj Delipetrov, European Commission Joint Research Centre, Italy
Zoran Zdravev, Faculty of Computer Science, UGD, Republic of North Macedonia
Aleksandra Mileva, Faculty of Computer Science, UGD, Republic of North Macedonia
Igor Stojanovik, Faculty of Computer Science, UGD, Republic of North Macedonia
Saso Koceski, Faculty of Computer Science, UGD, Republic of North Macedonia
Natasa Koceska, Faculty of Computer Science, UGD, Republic of North Macedonia
Aleksandar Krstev, Faculty of Computer Science, UGD, Republic of North Macedonia
Biljana Zlatanovska, Faculty of Computer Science, UGD, Republic of North Macedonia
Natasa Stojkovik, Faculty of Computer Science, UGD, Republic of North Macedonia
Done Stojanov, Faculty of Computer Science, UGD, Republic of North Macedonia
Limonka Koceva Lazarova, Faculty of Computer Science, UGD, Republic of North Macedonia
Tatjana Atanasova Pacemska, Faculty of Computer Science, UGD, Republic of North Macedonia

CONTENT

Balkan Journal of Applied Mathematics and Informatics
Volume V Number 1 Year 2022
Online ISSN 2545-4803
UDC: 621.313.333.072.9:519.876.2

REVIEW OF THE SCALAR CONTROL STRATEGY OF AN INDUCTION MOTOR: CONSTANT V/f METHOD FOR SPEED CONTROL

MARIJA STERJOVA AND VASILIJA SARAC

Abstract. This paper presents the design, simulation, and analysis of the speed control of an induction motor powered by a voltage inverter with a pulse-wide modulation method. The derived model addresses issues related to the regulation of motor speed at various supply frequencies. The control strategy of the voltage inverter is based on the scalar control with a constant V/f ratio, which is important for automated control, controlled start-up, acceleration and stop, and constant flux operation of the motor. The Powersim software is used for the purposes of deriving the simulation model in this paper. The analysis of the output results compares the different speeds of operation, below and above the nominal speed of the motor. They are also compared with the theoretical calculations required for the simulation model.

1.Introduction

Globally, electric motors are widely used in all fields of application and are essential to our present lifestyle. The technology of variable speed drives is highly valued and necessary for many aspects of production. This technology has a wide range of implementation in industrial applications and is crucial for any movement in periods - when and where everything is required. In addition, the indicated technology is extremely significant when dealing with the induction motor in response to the sophistication of factory automation that provides improved productivity. Furthermore, it overcomes the only drawback of the induction motor, the inability to operate at variable speeds. This technology includes voltage inverters and various modulation techniques that enable motor speed control. An asynchronous motor with a squirrel cage rotor is the preferred option due to its simple design, less maintenance, and simple operation. There are two basic control strategies used to control the speed of squirrel-cage induction motors: scalar and vector control strategies. Scalar control strategy is a relatively simple control method. The purpose of the technique is to control the magnitude of the chosen control quantities. Vector control strategy is a more complex control technique, the evolution of which was inevitable, too, since scalar control cannot be applied for controlling systems with dynamic behavior [1]. The vector control strategy works with vector quantities that have both the magnitude and the direction, respectively, named as space phasors. It is additionally known as field-oriented control.

Common control methods are classified as: changing the number of stator poles, varying supply frequency, variable rotor resistance, variable stator voltage, slip compensation, method of constant V/f ratio, vector control, etc. Scalar control schemes may be adequate in variable speed applications where speed disturbance is load tolerant. In this paper, the Powersim software simulates a three-phase squirrel cage induction motor model with a given output power of 0.55 kW, which uses the V/f control method. This control principle requires that the frequency and voltage applied to the stator of the motor have a constant ratio for the rated and below the rated speed.

Date: April 2022.
Keywords. Scalar control strategy, Speed control, Induction motor, Constant V/f control method, Powersim.

Above the rated speed, the motor enters a so-called flux weakening region, since the frequency is increased while the voltage is limited with the voltage of the DC bus link of the invertor. This means that the rise in frequency and voltage is no longer proportional, so consequently the motor flux is weakened as well as the available torque of the motor. The simulation characteristics are analyzed under different conditions because of different speeds, at, above, and below the nominal speed.

2. Theoretical background of the Variable Frequency Drive and the Constant V/f Control Method

In this section of the paper, the theory of the variable frequency drive (VFD) and the constant V/f control method will be reviewed.

2.1 Variable Frequency Drive

A variable Frequency Drive is a type of device that reliably and cost-effectively causes an AC motor to run at different speeds. A VFD is also termed as an AC drive, an inverter, an adjustable frequency drive, or an adjustable speed drive.

In Figure 1, a schematic diagram of the VFD is represented with the main components of the drive. The components, as well as the principle of operation, are explained below. Clearly, we can see from the schematic that the VFD includes:

-Input power – AC voltage comes into most drives. It enters the rectifier circuit.

-Rectifier Circuit – Bridge rectifier, which is a group of six diodes that convert AC to DC. In this form the DC voltage is still not smooth and has some ripple.

-DC Bus – A DC Bus system is in place usually with a capacitor and helps smooth out the ripple [10,12,13].

-Inverter Circuit – The DC current follows along with a group of switches of transistors that open and close to allow for positive or negative voltage output. This presents a PWM voltage pulse in a square shape. Since it is done multiple times with varying the degrees, the square-shaped pulse will increase and decrease in width. The AC motor interprets this as an AC sinusoidal current waveform and moves as if it were such. By increasing or decreasing the pulse width through the drive, the AC motor responds.

-IM – Induction motor.

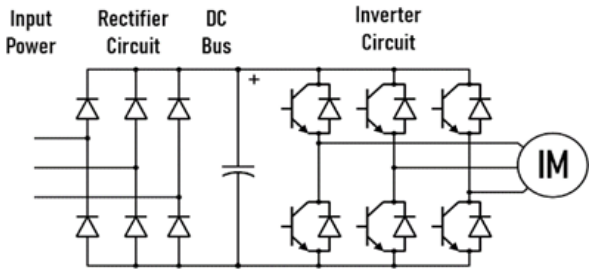

Figure 1. Representation of PWM VFD schematic diagram

The main task of the Variable Frequency Drive [2]:

1. VFD (AC drives) are used for step-less speed control of squirrel cage induction motor mostly used in process plants due to its ruggedness and maintenance-free long life.
2. VFD controls the speed of a motor by fluctuating yield voltage through a complex microchip-controlled hardware device.

The Variable Frequency Drive is a completely practical straightforward drive that allows acceleration of the motor up to the required speed. However, motor speed is limited due to the construction of the motor itself. Most often, the upper limit of the speed is limited to 1.5 times of the rated speed as the motor temperature increases at higher speeds and gives rise to potentially hazardous situations due to the high temperature and mechanical limitations imposed by the motor frame and bearings.

2.2 Constant V/f control method

Induction motors are three-phase machines where, the synchronous speed, also known as the speed of the revolution of the magnetic field in the stator winding of the motor n_s (rpm), is represented by the expression:

$$n_s = \frac{120*f}{p} \tag{1}$$

where, p is the number of poles, and f (Hz) is the frequency of the applied voltage waveforms. From this we can say that the synchronous speed as well as the rotor speed can be controlled by varying the frequency. If we vary the supply frequency, the synchronous speed can be varied, and if the synchronous speed is varied, it can directly affect the motor speed.

The expression of ratio $V/f = const$ is represented as follows:

$$E = V = 4.44\, f \phi_m k_n N \quad \rightarrow \quad V/f = 4.44\, \phi_m k_n N = const \tag{2}$$

where, V (V) is the voltage; ϕ_m (Wb) is the magnetizing flux; k_n is the winding constant, and N is the number of turns. The relation between the output power P (kW) and the torque T (Nm) is given by:

$$P = T \cdot \omega \tag{3}$$

where, the angular velocity, ω (rad/s) is defined by:

$$\omega = 2\pi f \tag{4}$$

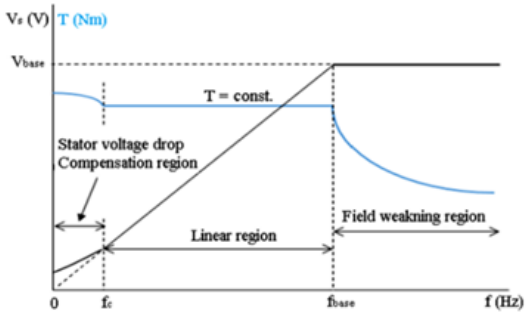

Figure 2. Stator voltage versus frequency at the V/f control method [5]

If the speed changes, it is observed that the maximum torque of the motor becomes constant when the constant V/f ratio is maintained [5]. The flux produced is in proportion to the ratio of the voltage applied and the supply frequency. Also, the motor developed torque is in direct proportion to the stator produced magnetic field [3]. Over the entire speed range, the magnetic flux and torque values can be kept constant with the same ratio of voltage and frequency variation [6, 10]. Figure 2 shows a graphic of the open loop V/f control method of an induction motor. A more detailed overview of the open loop V/f control method can be found in [3, 4]. As we can see, there are three frequency regions [5,6,7]:

- $0 - f_c$, the voltage drop across the stator resistance that cannot be neglected and must be compensated for by increasing the stator voltage. The torque in this frequency range is significantly higher (especially at zero speed).
- $f_c - f_{base}$, it follows the constant V/f relationship. The slope in fact represents the air gap flux quantity.
- $> f_{base}$, the stator voltages would be limited at the rated value to avoid insulation breakdown at the stator windings and the air gap flux would be reduced and cause the decreasing developed torque correspondingly.

From the above we can conclude that when frequency rises, the stator voltage is also increased, but above the base frequency the value of the stator voltage must be kept constant. In terms of output power and torque, it follows that up to the base speed the value of the torque is constant due to the constant ratio of V/f; after the base frequency the torque is reduced. In the second frequency region characterized by constant torque, the rise of frequency gives rise to the output power of the motor. While in the third frequency region for the values of the frequency above the base frequency, the output torque of the motor decreases, and due to the frequency rise and the decrease of the output torque, the value of the power $P=T\cdot\omega$ is maintained constant. This V/f control method is used for the model presented in this paper.

3. Simulation model

In Figure 3 the simulation diagram of the open loop V/f control of three-phase IM is shown. More precisely, this diagram contains the VFD – system as a model, as previously stated.

There are four main sub-units of the system:

1. **Three-phase bridge rectifier** with diodes,
2. **DC voltage link** with an inductor and a capacitor.
3. **Voltage Source Invertor** (VSI) that serves for power supply and contains an **Insulated-Gate Bipolar Transistor** (IGBT) with six switches IGBT1 - IGBT6 and
4. **Pulse Width Modulation** (PWM) technique that manages IGBT and operates with a series of pulses "ON-OFF" and changes the working cycle.

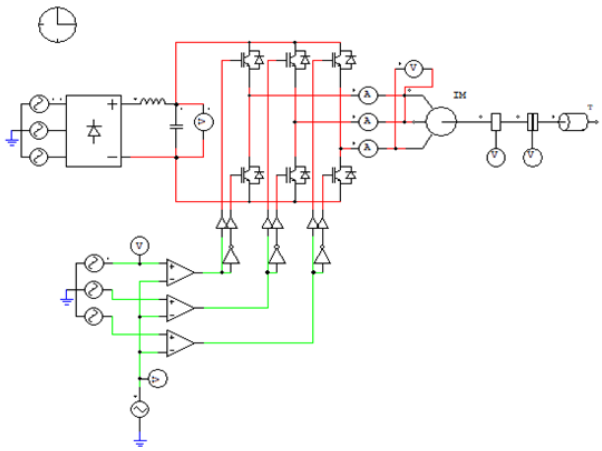

Figure 3. Simulation diagram of V/f speed control of induction motor

The output of the VSI inverter, based on 6 IGBT switches, is controlled using PWM (Figure 3), which allows to control the speed. This is due to the points at which the triangular carrier signal intersects with the sinusoidal modulation signal. The variation of the frequency and amplitude of the modulation signal provides the different operating speeds of the motor [11, 13]. Table 1 provides rated data and parameters used for V/f speed control of three-phase induction motor fed by voltage inverter.

Table 1. Rated data and parameters used for V/f speed control of induction motor

Rated data and parameters	Value
Output power P_2 (kW)	0.55
Rated Voltage (V)	400
Rated Current (A)	1.6
Rated Speed (rpm)	1,390
Rated Torque (Nm)	3.8
Number of Poles	4
Operating Temperature (°C)	75
Starting current (A)	4
Power factor or displacement factor DF (/)	0.74
Efficiency η (%)	0.67

4. Results and discussion

The design and construction of the model of this motor are intended for operation with a rated speed of 1,390 rpm and a rated load of 3.8 Nm. The results will be presented for three operating modes: at base speed, above and below the base speed. In the first two cases, the motor will be loaded with a rated load with the load of 3.8 Nm, while in the third case the motor will be in the field weakening and the load torque will be reduced as the motor cannot be accelerated anymore with the rated torque. The motor torque, current and speed will be presented as transient characteristics during motor acceleration and when it reaches steady-state operation at different speeds. The obtained results from transient characteristics of current, speed and torque will be compared with the data from the calculation and the motor data presented in Table 1.

4.1 Simulation results obtained at rated frequency

In the initial analysis, the frequency of the sinusoidal modulating signal is set to a rated frequency of 50 Hz and the motor is loaded with a 3.8 Nm constant load. Figure 4 presents the transient characteristics of speed, torque, and current as a function of a rated supply frequency of 50 Hz. In accordance with the data in Table 1 and the charts in Figure 4, it can be assumed that the starting torque of the motor is sufficiently large to allow the acceleration of the motor to the rated speed. From the graph in Figure 4 (a), we can see that after acceleration with a constant load of 3.8 Nm and moment of inertia of 0.001 kgm^2, the motor reaches a speed of 1,330 rpm. This value corresponds to the analytical

value obtained from the calculations and analyses (Table 1). The result (b) also shows that the output torque reaches 3.8 Nm after motor acceleration. And this result is expected as well, if we consider that the motor is loaded with 3.8 Nm. When operating in steady state, the RMS value of the current is 1.4 A, corresponding to the current with a rated value of 1.6 A.

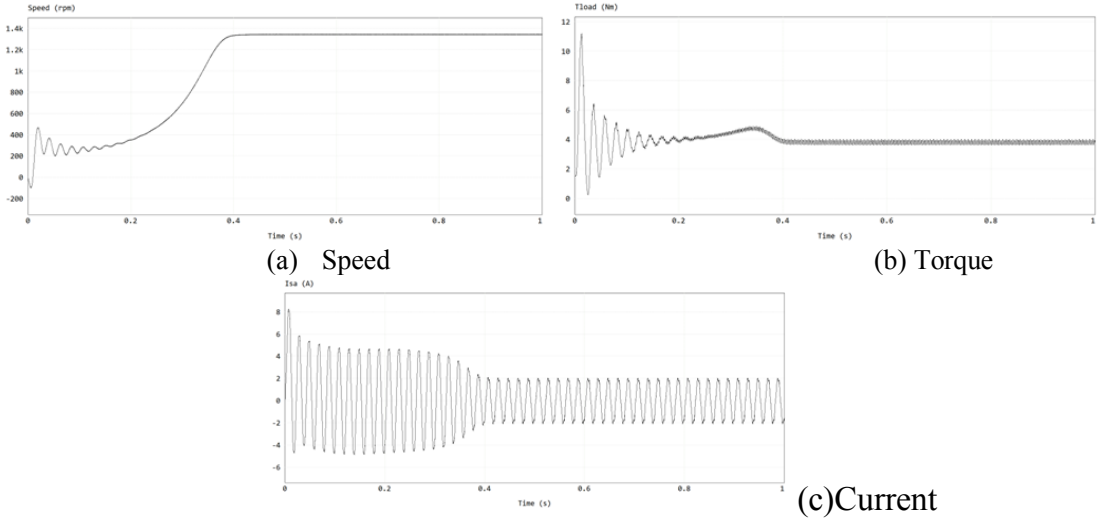

(a) Speed (b) Torque (c)Current

Figure 4. Transient characteristics of speed, torque and current at 50 Hz

Additionally, the motor is operating with a power converter. This means that the power factor of the motor is not just the phase displacement between voltage and current as it is usually calculated from the formula:

$$PF_D=P/S \tag{5}$$

Where P is the motor active power in W, and S is the apparent power in VA.
Due to the presence of the higher order harmonics which are fed into the motor power supply by the power converter, the true power factor can be calculated as:

$$PF_T=PFD \cdot DF \tag{6}$$

Where DF is the distortion power factor, and it can be found from:

$$DPF = \frac{1}{\sqrt{1+THD^2}} \tag{7}$$

Where, THD is the total current harmonic distortion. Further details can be found in [14]. Therefore, two more measurements were done on the input power supply of the motor: the apparent power and the power factor. They are presented in Fig. 5 (a) and (b) respectively.

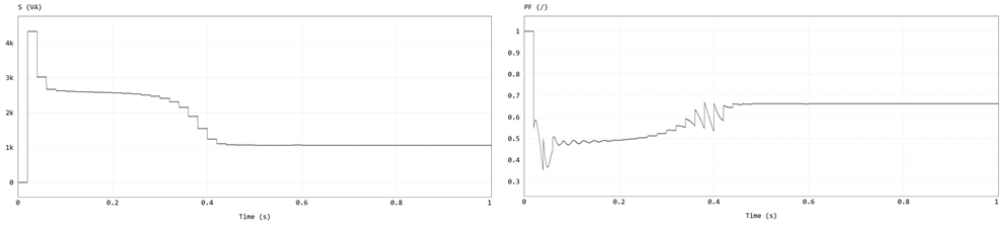

(a) Apparent power (b) Power factor

Figure 5. Transient characteristics of apparent power and true power factor at 50 Hz

From the presented results in Fig. 5, it is obvious that the power factor is lower than the power factor presented in Table 1. In the simulation circuit 0.67 versus 0.74 is measured, presented in Table 1 from the data of the producer. The exact measurement of the power factor depends on the accurate calculation of the motor parameters, especially inductances, stator rotor, and magnetizing inductance. Here it should be noted that the entered parameters in the simulation model are calculated based on the data from the experiments, i.e., approximately. The exact calculation of motor parameters is subject to further research and analysis in different software programs. Furthermore, the measured power factor in the simulation circuit is the displacement factor PF_D. As the current distortion is not so pronounced, the THD is assumed to be negligible.

Another issue is motor efficiency. It will be lower than the value presented in Table 1 (67 %). The reason is the presence of higher order harmonics that will cause additional copper losses. We will assume only the third and fifth harmonics are present in the current wave form. This will cause additional copper losses of 12 W. Therefore, motor efficiency (η) will decrease from 66%. The measured apparent power from Fig. 5 (a) is approximately 1,050 W. According to the data in Table 1, the apparent power of the real motor is 1,107 W for the same motor loading 3.8 Nm. Therefore, the simulation model can be considered sufficiently accurate. The motor input power when it is supplied by a converter is 703 W (P_1) and it is calculated from:

$$P_2=P_1\cdot\eta \tag{8}$$

The motor output power is now 463 W. This means that the motor torque is calculated from:

$$T=9.55\cdot(P_2/n) \tag{9}$$

Where n is the motor speed in rpm, i.e., 1,330 rpm. The rated motor torque in case when the motor is supplied from the inverter at 50 Hz will be 3.3 Nm according to measured and calculated data. In our model, the motor is loaded with 3.8 Nm for the inertia of 0.001 kgm^2. Loading the motor with a bigger torque than 3.8 Nm is not possible. The calculated value of 3.3 Nm corresponds well with the obtained result of the torque from the simulation. The difference in the results (3.3 Nm and 3.8 Nm) comes from the motor parameters and accurate calculation of motor efficiency. Motor parameters are entered into the model, based on the calculations from the motor experimental measurements. The exact calculation of the motor parameters is part of another analysis, and it is done with another software program.

The inverter DC link voltage and current are presented in Fig. 6 (a) and (b).

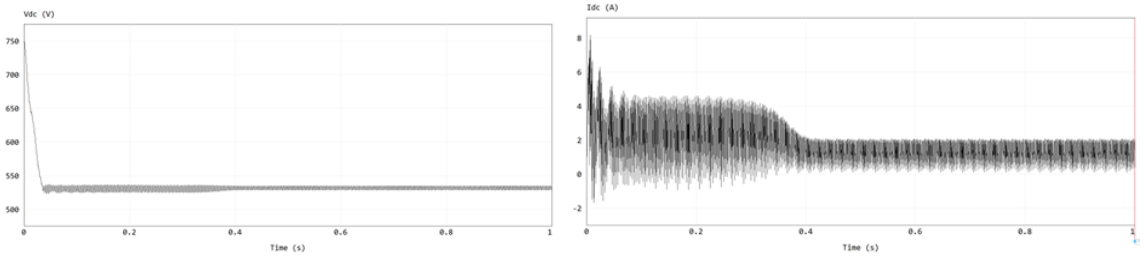

(a) Voltage (b) Current

Figure 6. DC link voltage and current

The DC link current can be calculated from following formula:

$$DC_{linkpower} = V_{DC} I_{DC} = \frac{AC_{poweroutput}}{\eta} \quad (10)$$

V_{DC} is the link voltage, I_{DC} is the link current. $AC_{poweroutput}$ is the load of the inverter in W, and η is the inverter efficiency. So, for our analysis $AC_{poweroutput}$ is 703 W; inverter efficiency is assumed to be 0.95. Exact calculations of inverter efficiency are out of the scope of this paper. Therefore, the $DC_{linkpower}$ is 668 W. From Fig. 6 (a), the DC link voltage is 530 V. The calculated DC link current is 1.3 A. The presented DC link current in Fig. 6 (b) has the RMS value of 1.4 A when the motor reaches steady-state operation.

4.2 Simulation results obtained when the motor is operating below the rated speed

In case of motor operation below the rated speed, the frequency of the sinusoidal modulating signal is reduced to 25 Hz and the motor is running at low speed at a rated load of 3.8 Nm. Simulated transient characteristics of speed, torque, and current are obtained, and are presented in Figure 8. From the graph shown in Figure 8 (a), we notice that after acceleration of the motor, loaded with 3.8 Nm, it achieves a speed below the rated, approx. 700 rpm. According to equation (1), which determines the synchronous motor speed with a supply frequency of 25 Hz, it is expected that the speed value will be less than 750 rpm after the motor accelerates. The result (b) shows the output torque reaching 3.8 Nm after motor acceleration. The motor is not operating in a flux weakening region, so it can accelerate with a rated load of 3.8 Nm following the rule V/f=const. As for the current, it varies with the variation in speed and torque. When the motor is running below the rated speed, the current also decreases. The ratio of the current reduction due to the variation in speed and load is presented in Fig. 7. According to Fig. 7, the reduction of 58 % of the current is expected when the motor is operating at 0.5 times the rated speed and with the rated load. As a last one for this case, result (c) shows that the motor current is reduced to 0.95 A (RMS value), which corresponds to the expected value of 0.928 A i.e., a 58 % reduction of the rated current of 1.6 A, obtained for the operation with 50 Hz and rated load.

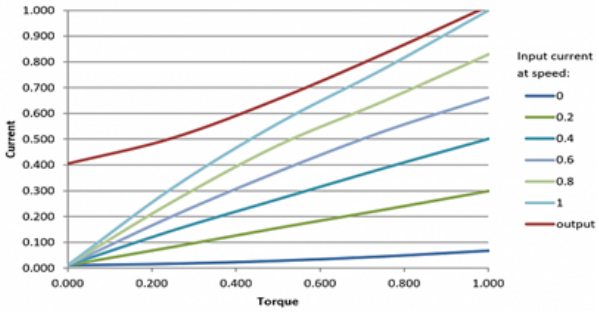

Figure 7. Variation of drive input current with torque and speed [15]

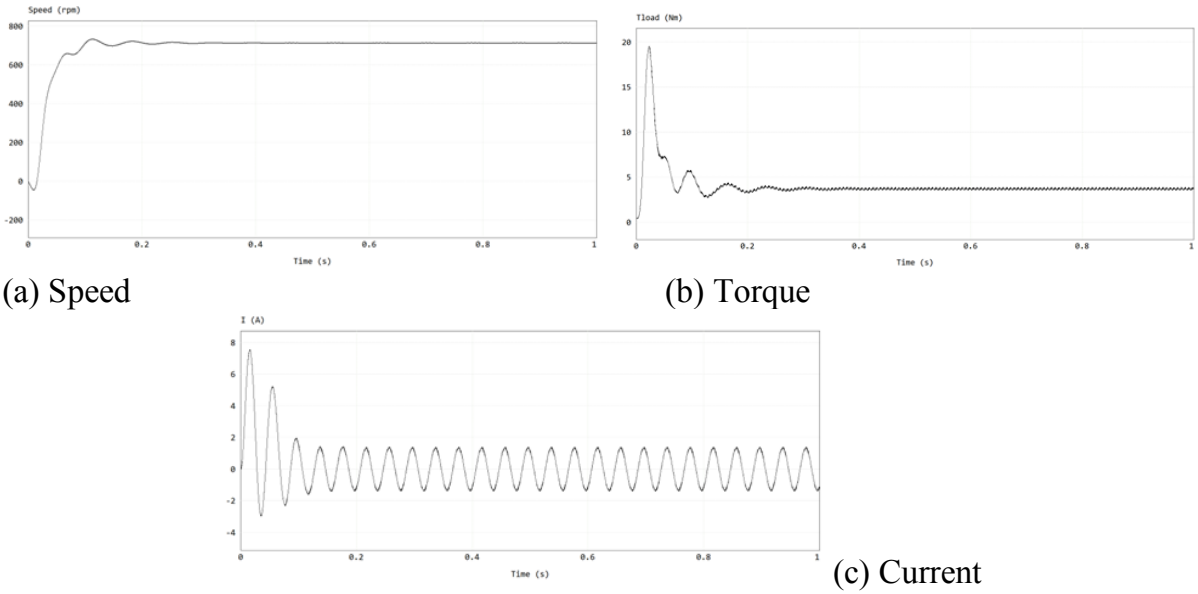

(a) Speed (b) Torque

(c) Current

Figure 8. Transient characteristics of speed, torque and current at 25 Hz

The measured load of the output of the inverter, in this case, is 730 VA; the power factor is 0.48; and the input power of the motor is 350 W. This can be expected as the motor is operating in the linear region of P-characteristic below the base speed (Fig. 2). The efficiency is 0.66 of the motor (as it is for the supply 50 Hz with the inverter) so the motor output mechanical power P_2 is 231 W. According to formula (9) for the speed of 700 rpm, the motor torque is 3.2 Nm. The motor is loaded with 3.8 Nm in the model for 25 Hz and moment of inertia of 0.001 kgm^2 (Fig. 8 (b)). Again, the difference in motor torque (3.2 Nm and 3.8 Nm) is a result of the accuracy in calculation of the motor parameters which must be input in the motor model. The measured apparent power and power factor are presented in Fig. 9 (a) and 9 (b) respectively.

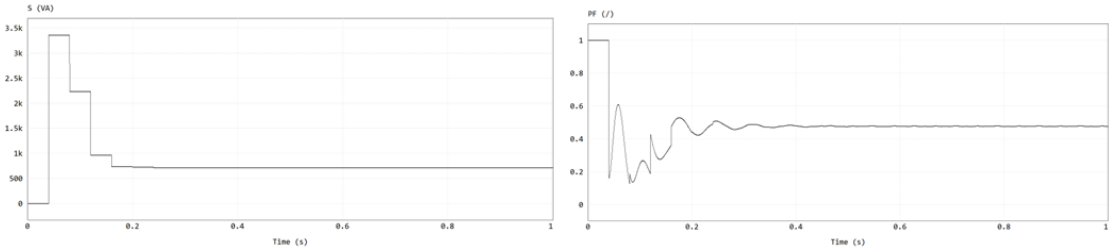

(a) Apparent power (b) Power factor

Figure 9. Transient characteristics of apparent power and power factor at 25 Hz

4.3 Simulation results obtained when the motor is operating above the rated speed

In the analysis of the third case, the frequency of the sinusoidal modulating signal is increased above the nominal frequency by 75 Hz. When the motor is operating above the rated speed, the torque decreases, and the motor enters the field-weakening region following the control rule V/f=const, i.e., frequency is increased while the supply voltage of the motor remains unchanged due to the converter limitations. This applies when the motor is running with a constant flux. Figure 10 represents simulation graphs of speed, torque, and current.

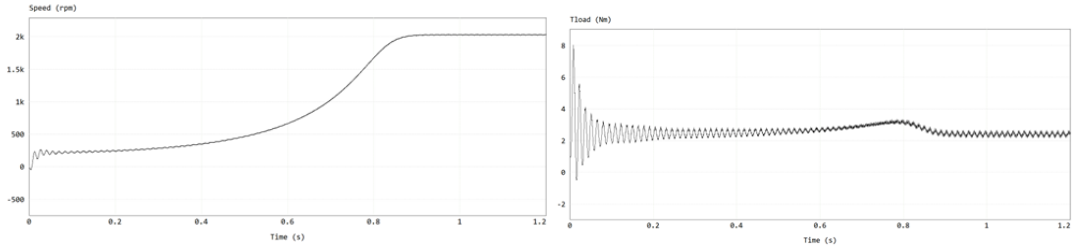

(a) Speed (b) Torque

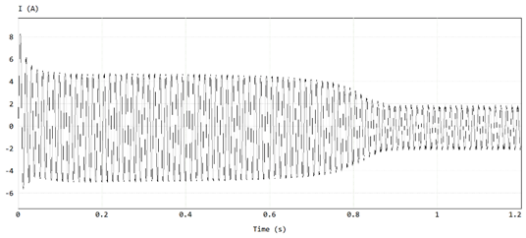

(c) Current

Figure 10. Transient characteristics of speed, torque and current at 75 Hz

According to equation (1) the expected value of the motor synchronous speed is 2,250 rpm at a frequency of 75 Hz. The resulting motor speed value in Figure 10 (a) is approximately 2,000 rpm and it corresponds to the expected value of the loaded motor. A decrease in torque from the rated value of 3.8 Nm to a value of 2.4 Nm is observed in the result (b), at a 1.5 times higher frequency. One example of what the ranges of reduction of motor torque are can be found in [15]. They are presented in Fig. 11. According to Fig. 11, at the 1.5 times the rated frequency, a torque reduction of 64 % is expected, or for a rated torque of 3.8 Nm the torque reduction is 2.4 Nm. The obtained result in Fig. 10 (b) presents the torque reduction 2.4 Nm. The acceleration time of the motor increases, when the motor is running in the flux weakening region. The motor current after the acceleration time is finished, is reduced up to the rated current, as the motor operates with constant power and constant voltage, in the flux weakening region.

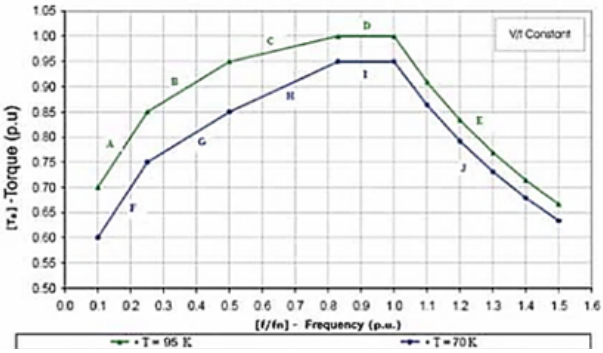

Figure 11. Torque reduction for constant flux operation [16]

The apparent power and true power factor are measured for this case as well. They are presented in Fig. 12 (a) and (b) respectively.

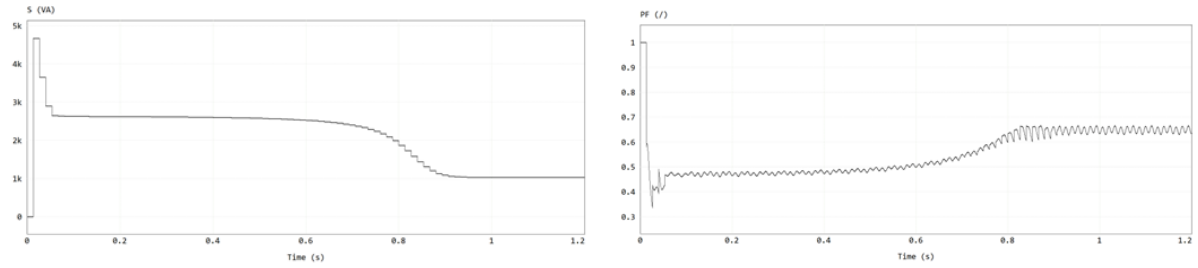

(a) Apparent power (b)Power factor

Figure 12. Characteristics of apparent power and true power factor at 75 Hz

The motor operates at constant power region. The loading of the inverter is the same as it is at a 50 Hz power supply, i.e., 1,000 VA with the power factor of 0.65. The motor losses of the motor are increased due to the increased frequency, which means increased iron losses i.e., eddy current losses. The iron core losses increased from 28.17 W to 40.7 W. The motor efficiency is 0.66. The output mechanical power P_2 is 429 W and the motor torque for a speed of 2,000 rpm is 2 Nm. The motor is accelerated with a torque of 2.4 Nm (Fig. 10 (b)). This is the largest torque with which the motor can be accelerated. The further increase of torque results in unsuccessful starting of the motor.

5. Conclusion

In this paper, a scalar control strategy has been reviewed. This strategy is based on the linearization of the non-linear IM equations at operating points in the stable state. Scalar control is the most popular form of control of AC drives, because of its low cost and ease of use, especially in open loop mode. It is obtained by controlling the stator voltage and frequency, therefore maintaining the air-gap flux of the motor constant. The addition of a VFD to a three-phase induction motor makes it possible to control the speed of the motor, depending on the load of the motor, which saves energy. VFD is the most efficient system to control the speed of the IM by varying the supply frequency and keeping the V/f ratio constant. This results in a control scheme with a wide speed range of operation that also improves the starting performance of the motor and provides good steady-state operation of the motor as well. With the development of the simulation model in Powersim, as presented in section 4, results are obtained under different conditions: at, below, and above the rated speed of the motor. In the analysis of these results, values are also compared to the values of the theoretical model and analytical calculations. This presented simulation model is a useful tool for simulation and examination of induction motor drive systems operating at various speeds, especially when there is no adequate laboratory equipment available.

References

[1] *G. Kohlrusz, D. Fodor* (2011). "Comparison of scalar and vector control strategies of induction motor". Hungarian journal of industrial chemistry VEZPRÉM. Vol. 39(2) pp. 265-270.

[2] *B. Sourabh, P. Darshan, S. Rupesh, N. Ghuge* (2020). "Application of VFD For Three Phase Induction Motor". ICCIP. Department of Electrical Engineering BSIOTR, Wagholi, Pune-412207, India.

[3] *Bharti, Ranju; Kumar, Madhav; Prasad, B.M* (2019). "V/F Control of Three Phase Induction Motor". International Conference on Vision Towards Emerging Trends in Communication and Networking (ViTECoN), Vellore, India. pp. 1-4.

[4] *Mr. P. Kondibarao Hingmire , Mr.S. Kumar Rayarao* (2016). "Development of a V/f Control scheme for controlling the Induction motor-both Open Loop and Closed Loop using MATLAB". International Journal of Scientific Engineering and Applied Science (IJSEAS) – Volume-2, MSSCET, JALNA, INDIA. pp. 403-407.

[5] *Z. Bala Duranay, H. Guldemir, S. Tuncer* (2020). "Implementation of a V/f Controlled Variable Speed Induction Motor Drive". EMITTER International Journal of Engineering Technology. Vol. 8, No. 1. pp. 35-48.

[6] *S. Osmanaj, K. Simnica Aliu, M. Limani, Q. Kabashi* (2018). "The sensitivity of the hoist system in crane applications from speed control methods at induction motor".

[7] *What-when-how.*: TORQUE-SPEED CHARACTERISTICS – CONSTANT V/F OPERATION (Motors and Drives), http://what-when-how.com/motors-and-drives/torque-speed-characteristics-constant-vf-operation-motors-and-drives/

[8] *Derouich, A., & Lagrioui, A.* (2014). "Real-time simulation and analysis of the induction machine performances operating at flux constant". International Journal Advanced Computer Science and Applications, 5, 59–64.

[9] *Jannati, M., Anbaran, S. A., Asgari, S. H., Goh, W. Y., Monadi, A., Junaidi, M. A. A., & Idris, N. R. N.* (2017). "A review on variable speed control techniques for efficient control of single-phase induction motors: Evolution, classification, comparison". Renewable and Sustainable Energy Reviews, 75, 1306–1319.

[10] V. Shilpa, Kailaswar, Prof. R.A.Keswani (2013). "Speed Control of Three Phase Induction Motor by V/f Method for Batching Motion System". International Journal of Engineering Research and Applications (IJERA). Vol.3, Issue 2. pp.1732-1736.

[11] *V. Sarac, G. Stefanov, D. Minovski* (2021). "Speed regulation of induction motor with PWM inverter". International conference ETIMA, Vol 1. pp. 30-41.

[12] *Frederick D. Kieferndorf, Member, IEEE, Matthias Förster, and Thomas A. Lipo* (2004). "Reduction of DC-Bus Capacitor Ripple Current With PAM/PWM Converter". IEEE TRANSACTIONS ON INDUSTRY APPLICATIONS, VOL. 40, NO. 2. pp.607-614.

[13] M. Ahsan Niazi, Q. Hayat, B. Khan and M. Afaq (2020). "Speed control of Three Phase Induction Motor using Variable Frequency Derive Control System". International Journal of Current Engineering and Technology. Vol. 10, No.1.

[14] W. Grady and R. Gilleskie, "Harmonics and How They Relate To Power Factor," Proc. of the EPRI Power Quality Issues & Opportunities Conference (PQA'93), San Diego, CA (1993), pp. 1-8.

[15] Technical: "Current, power and torque in variable speed drives", 2017, available at: https://www.theautomationengineer.com/technical/current-power-torque-variable-speed-drives/.

[16] Weg "Induction motors fed by PWM frequency inverters", Technical guide, 2009.

Marija Sterjova
Goce Delcev University,
Faculty of Electrical Engineering,
Stip, Republic of North Macedonia
marija.22512@student.ugd.edu.mk

Vasilija Sarac
Goce Delcev University,
Faculty of Electrical Engineering,
Stip, Republic of North Macedonia
vasilija.sarac@ugd.edu.mk